Solar Energy Materials and Solar Cells 168 (2017) 51–61

Contents lists available at ScienceDirect

Solar Energy Materials and Solar Cells

journal homepage: www.elsevier.com/locate/solmat

Potential induced degradation of N-type bifacial silicon solar cells: An investigation based on electrical and optical measurements

M. Barbato[a,b,*], A. Barbato[a], M. Meneghini[a], G. Tavernaro[c], M. Rossetto[d], G. Meneghesso[a,b]

[a] Department of Information Engineering, University of Padova, Via Gradenigo 6/B, 35131 Padova, Italy
[b] Centro Levi Cases, University of Padova, Via Marzolo 9, 35131 Padova, Italy
[c] MegaCell S.r.l., Via Postumia Vecchia 9, 35010 Carmignano di Brenta, Padova, Italy
[d] MRP S.r.l., Via Del Cristo 378, 35100 Padova, Italy

ARTICLE INFO

Keywords:
Photovoltaic N-type solar cells
Reliability
Potential induced degradation
Electroluminescence
External Quantum Efficiency

ABSTRACT

This paper reports an extensive analysis of the potential-induced degradation (PID) of N-type bifacial solar cells. The analysis is based on combined electrical characterization, electroluminescence and external quantum efficiency measurements, carried out on solar cells submitted to high PID stresses. We investigate the impact of two different encapsulation materials: (i) polyolefin elastomer (POE) and (ii) ethylene-vinyl-acetate (EVA). We describe the degradation and recovery kinetics as a function of the temperature and the stress voltage. Moreover we demonstrate that the POE can be adopted to reduce the decrease of conversion efficiency during PID stresses. Finally we investigate the effects of PID with an optical analysis in order to find the main cause of the performance degradation.

1. Introduction

In the last years, monocrystalline N-type bifacial silicon solar cells have received attention due to their higher efficiency with respect to p-type solar cells [1]. The primary motivation for the better performance is related to the higher tolerance to transition metal impurities [2]. The higher performance compared to p-type solar cells have been thoroughly studied and demonstrated [3–5]. In 2015 the market of monocrystalline n-type solar cells was limited to less than 7% but it is expected to grow up to 30% before 2025 [6].

Despite the excellent technological advances, several factors may favor the degradation of solar cells during long-term operation, including: (i) the decrease in shunt resistance of the single solar cells due to the generation of hot spots [7,8], (ii) the degradation of the encapsulants [9], (iii) light induced degradation (LID) [10,11], (iv) ambient related issues like humidity and temperature [12] and (v) potential induced degradation [13].

Potential induced degradation (PID) occurs when a large potential difference is applied between the solar cells (that can reach hundreds of volts in series-connected modules) and the grounded frame that surrounds the module, and may lead to a significant degradation of the electrical characteristics of the cells, and to a not negligible leakage current through the encapsulant material. PID was extensively studied on p-type silicon solar cells [14–16]. Only recently, some research groups tried to address the PID issue in n-type silicon solar cells [17,18]. The main cause of the PID degradation is not yet understood, and several explanations have been given so far in the literature: Naumann [19] associated the degradation of p-type solar cells subjected to PID to the presence of sodium (Na) in the active layers; Hara [17] and Swanson [20] explained the effects on n-type solar cells as due to an enhanced front surface recombination between electrons and holes; Halm [18] attributed the PID effects to a degradation of the front surface passivation; finally, Naumann [21] divided the PID effects into two categories: shunting potential induced degradation (PID-s) and degradation of the front surface passivation (PID-p).

The aim of this paper is to contribute to the understanding of the PID effects on the performance of monocrystalline n-type silicon solar cells. More specifically, we analyze: (i) the impact of the encapsulant material on PID robustness; (ii) the effect of four different temperatures (35 °C, 50 °C, 65 °C and 80 °C) and three different applied voltages (−300 V, −450 V and −600 V), by subjecting various solar panels to different PID stresses and recovery phases with a positive applied voltage; we extrapolated the Arrhenius plot of the temperature-dependent degradation, and we describe the dependence of the degradation kinetics on the applied voltage. (iii) In order to achieve a detailed description of the PID effects, we performed an optical analysis through electroluminescence (EL) and external quantum efficiency (EQE) measurements. The EL analysis allowed to identify two different

* Corresponding author at: Department of Information Engineering, University of Padova, Via Gradenigo 6/B, 35131 Padova, Italy.
E-mail address: barbatom@dei.unipd.it (M. Barbato).

http://dx.doi.org/10.1016/j.solmat.2017.04.007
Received 21 November 2016; Received in revised form 23 February 2017; Accepted 5 April 2017

degradation processes, a permanent one and a recoverable one. The results of the EQE measurements were related to the electrical measurements in order to investigate the recombination effects with varying incident wavelength. (iv) Finally, we performed and compared two PID stresses carried out with the aluminum sheet in the front side and in the rear side of a solar module in order to better explain the physical cause of the degradation induced by the PID on the performance of the solar cells.

2. Technology details

The study was carried out on $15.6 \times 15.6\ cm^2$ n-type bifacial solar cells, based on mono-crystalline silicon. The solar cells and mini-modules were manufactured by MegaCell s.r.l. using four busbars. MegaCell produces high efficiency solar cells up to 21% efficiency, with a bifacial factor > 88% (ratio between rear and front efficiency). The solar cell process has been developed and patented by the German ISC Konstanz Institute (ISC) and consists of a front alkaline texturing process with ozone cleaning, a front and back SiNx antireflection layer creation by PECVD, a double diffusion process (front BBr3 and rear POCl3), a laser edge isolation phase, a screen printing phase and a fast firing metallization process.

The cell architecture is schematically represented in Fig. 1a. In order to study the effect of the encapsulation on PID, two different materials were used: i) conventional good quality ethylene-vinyl-acetate (EVA) encapsulant with 450 μm thickness typically used for p-type cells lamination; ii) high quality pre-reticulated polyolefin elastomer (POE) film with 450 μm thickness and improved volume resistant properties. An extra clear 2 mm glass on the front side and a transparent back sheet on the back side have been used.

The 2 × 2 solar panels (Fig. 1b) have been soldered manually using standard ribbon SnPb 60/40 with dimensions 1.2 mm × 0.2 mm. For the lamination a one-step laminator has been used.

For the mini module assembly, the lamination recipe has been adjusted in order to obtain a minimum Gel content of 80%.

3. Experimental details

During the PID stress tests, the main cell parameters were monitored by means of (i) I-V measurements, both in dark condition and under illumination, (ii) electroluminescence characterization and (iii) external quantum efficiency measurements. The dark characterization was carried out by using a Keithley 2651 A source meter, programmed via LabView®. The characterization was carried out dynamically changing the current range in order to reach high accuracy in the current measurement from the microampere to ampere range. The light characterization was carried out by using the Keithley 2651 A and a microcontroller-based white LED solar simulator, properly calibrated and synchronized with the source meter. The solar simulator can produce different illumination levels from 0.2 suns up to 4 suns, by varying the current through the LEDs.

The electroluminescence images were carried out by using an InGaAs camera (Xenics), while biasing the solar cells or mini-modules with a forward current of 7 A. Finally the external quantum efficiency measurements were performed by using the commercial system LOANA (PV tools) with a light spot of 2 mm × 1 mm and a biasing light of 0.3 suns. The system is able to extrapolate the calibrated external quantum efficiency in the wavelength range between 300 nm to 1200 nm, and the map of the external quantum efficiency at fixed wavelength on a region of the solar cell. This system allowed to compare the EQE map signal with the EL signal extrapolated during the PID stress (see paragraph 4.3 for the results).

The stress experiments were carried out on 1-cell and 4-cells mini-modules, encapsulated by using POE and EVA. An aluminum sheet was applied on the front or back of the cells, to emulate the grounded frame of a real solar panel. The stress bias was applied between the (short circuited) solar cell and the aluminum foil, consistently with previous reports on the topic [22]. Degradation was induced as described in the following: after the preliminary characterization at 25 °C, the solar cell or module was subjected to a 1 h PID test @ −600V and 65 °C. Then the system was cooled down at 25 °C and the characterizations were carried out (dark and light IV, EL characterization and EQE characterization). This scheme was repeated for different steps with this cumulative timing: 1 h, 3 h, 7 h, 15 h, 39 h and 55 h. After the stress, a recovery phase @ +600 V and 65 °C for 48 h was applied with measurements at 24 h and 48 h in order to investigate the recovery of the PID stress.

This stress strategy allows to follow the evolution of the cell parameters (short circuit current I_{SC}, open circuit voltage V_{OC}, maximum power P_{MAX}, fill factor FF, series resistance R_S, shunt resistance R_{SH}, etc.) during the stress test and to investigate the failure point where the cells stop working properly. In particular, the EL can be monitored during the stress test, thus identifying the actual causes of failure.

4. Results and discussion

This paragraph is divided in 4 sections: Section 4.1 describes the electrical results of the PID stress @ −600 V for 55 h (T = 65 °C) and the related recovery phase @ +600 V for 48 h (T = 65 °C) performed on two bifacial solar cells encapsulated with two different encapsulants: (i) ethylene-vinyl-acetate (EVA-BSC) and (ii) polyolefin elastomer encapsulant (POE-BSC). Moreover the two diode model was used on the EVA-BSC cells in order to explain the nature of the degradation. Section 4.2 shows the results of the PID stresses carried out on a four solar cells module. In particular the stresses were performed at different voltages and at different temperatures in order to extrapolate the kinetics of the degradation. Section 4.3 shows the results of the optical analysis (electroluminescence (EL) and external quantum efficiency (EQE)). The correlation between the IV characterizations and the EL analysis was investigated. A physical motivation of the PID phenomena is given.

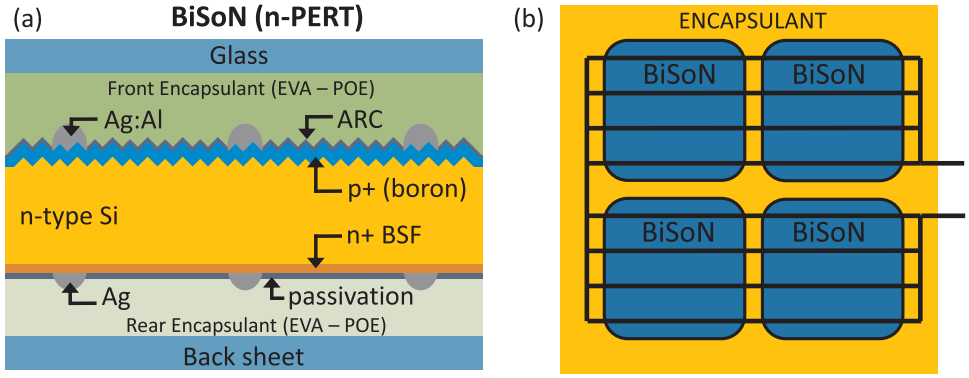

Fig. 1. (a) Cell architecture and (b) scheme of a 2 × 2 solar panel.

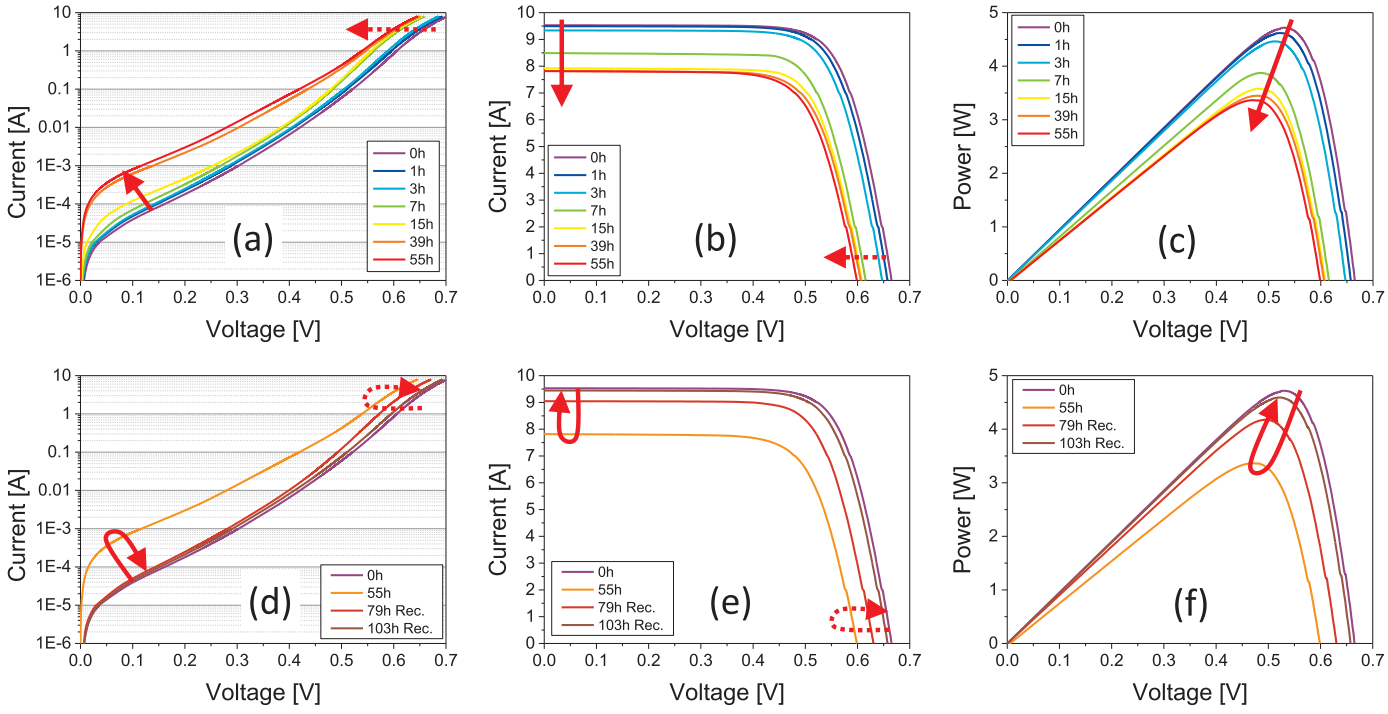

Fig. 2. Evolution of the dark current voltage (a, d), light current voltage (b, e) and power voltage (c, f) curves during the PID stress (a, b, c) and recovery (d, e, f) phases.

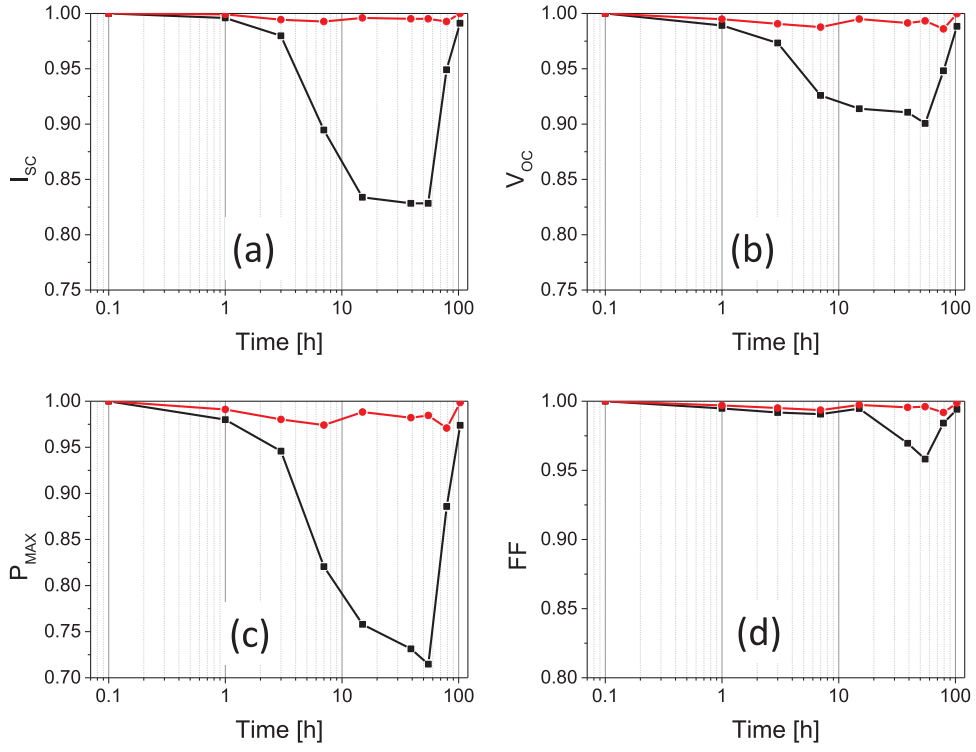

Fig. 3. Evolution of the short circuit current (I_{SC}) (a), open circuit voltage (V_{OC}) (b), maximum power (P_{MAX}) (c) and fill factor (FF) (d) during the PID stress and recovery phases for two BSCs with different encapsulation materials. (For interpretation of the references to color in this figure, the reader is referred to the web version of this article).

Finally the Section 4.4 shows the comparison of the PID stress applied on the front and rear faces of a solar module encapsulated with EVA. This allows to explain the nature of the degradation.

4.1. PID stress results: EVA and POE comparison

In Fig. 2 the electrical characterization of an EVA-BSC subjected to a PID stress @ −600 V for 55 h (T = 65 °C) and a recovery phase @ +600 V for 48 h (T = 65 °C) is shown. As can be noticed, during the stress phase the short circuit current and the open circuit voltage decrease significantly (see arrows in Fig. 2b). Moreover, the extracted maximum power decreases (see arrow in Fig. 2c). The shunt resistance (R_{SH}) decreases during the stress phase (see Fig. 2a), this is consistent with previous studies [22] which indicate the formation of micro shunt during the PID stress. During the recovery phase, the recovery is almost complete (see arrows in Fig. 2d, e and f). This allows to conclude that

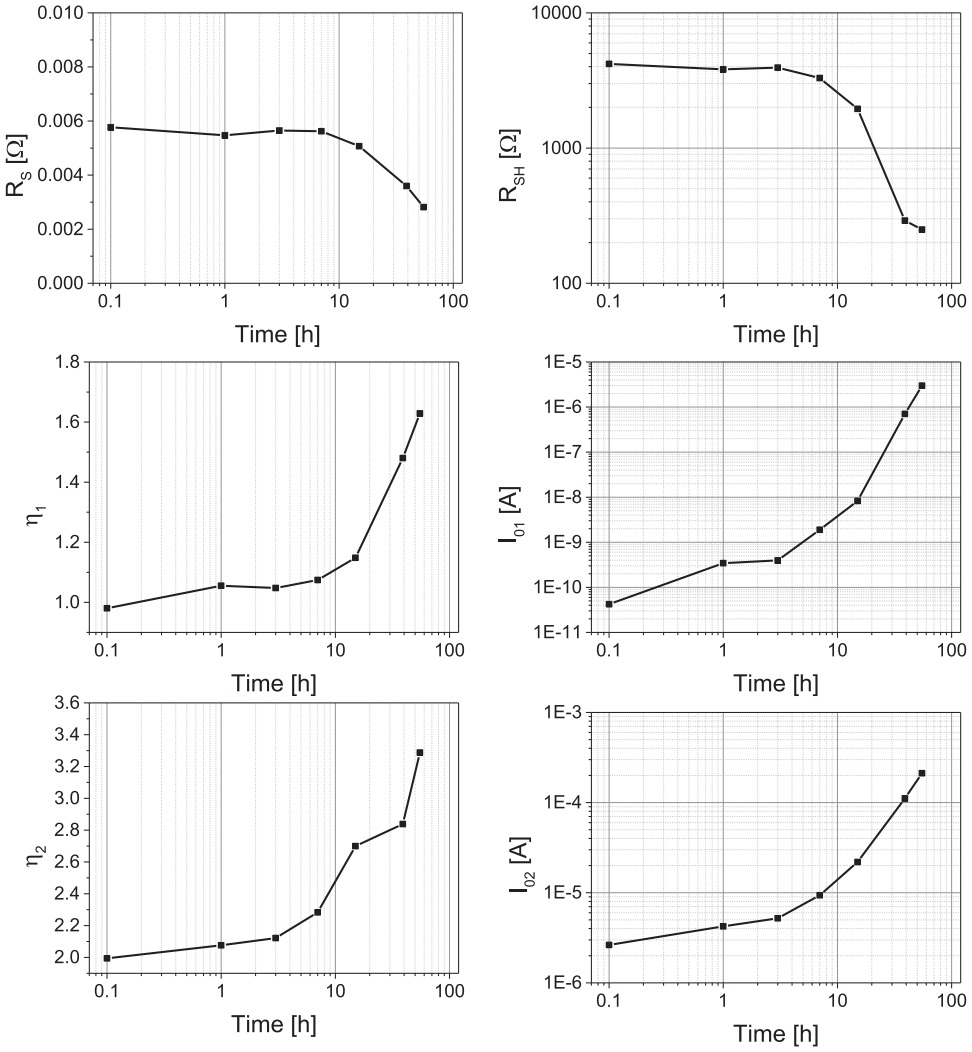

Fig. 4. Evolution of the two diode model parameters (R_S, R_{SH}, I_{01}, I_{02}, η_1 and η_2) during the PID stress @ −600 V for 55 h (T = 65 °C) on a EVA-BSC.

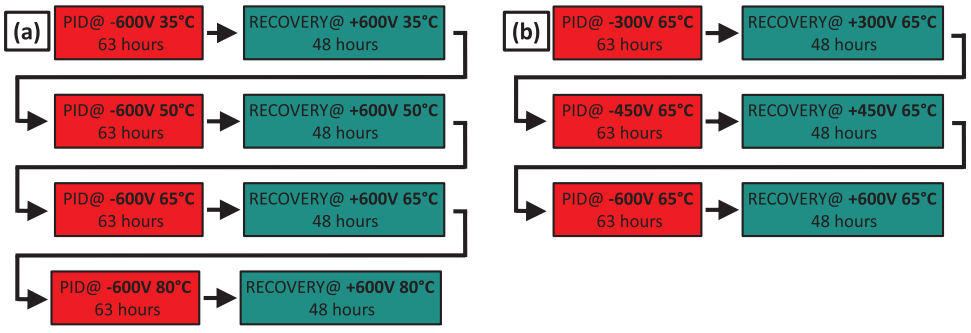

Fig. 5. Scheme of the two different stress procedures: (a) PID stresses and recovery phases at different temperatures and (b) PID stresses and recovery phases at different voltages. Each stress period is 63 h long and each recovery period is 48 h long.

the physical phenomenon of PID is mainly reversible.

For clarity, in Fig. 3 (black curves) we report the evolution of the short circuit current (I_{SC}), open circuit voltage (V_{OC}), maximum power (P_{MAX}) and fill factor (FF) during the PID stress and recovery phases extracted from the dark and light characterization of Fig. 2. The stress phase induces the lowering of the I_{SC} (Fig. 3a), the lowering of the V_{OC} (Fig. 3b), and the lowering of the P_{MAX} (Fig. 3c). All these parameters recover during the recovery phase. The FF decreases only after 15 h of PID stress, and recovers subsequently (Fig. 3d). In Fig. 3 the same parameters for a POE-BSC are presented (red curves). It can be seen that the use of a different material can result in a better robustness to PID. This is consistent with previous studies [23,24]. This can be related to major volumetric resistivity of the POE material ($> 10^{16}$ [Ω cm]) compared to the EVA material one ($> 10^{14}$ [Ω cm]).

We adopted the two diode model [25] as in [26] to the dark current voltage characterization of the EVA-BSC in order to extrapolate the evolution of the model parameters (series resistance, R_S, shunt resistance R_{SH}, dark saturation current of diode 1, I_{01}, dark saturation current of diode 2, I_{02}, ideality factor of diode 1, η_1, and ideality factor of diode 2, η_2) during the stress phase. Fig. 4 reports the results: the reduction of the shunt resistance, the increase of the dark saturation currents of the two diodes and the increase of the ideality factors can be

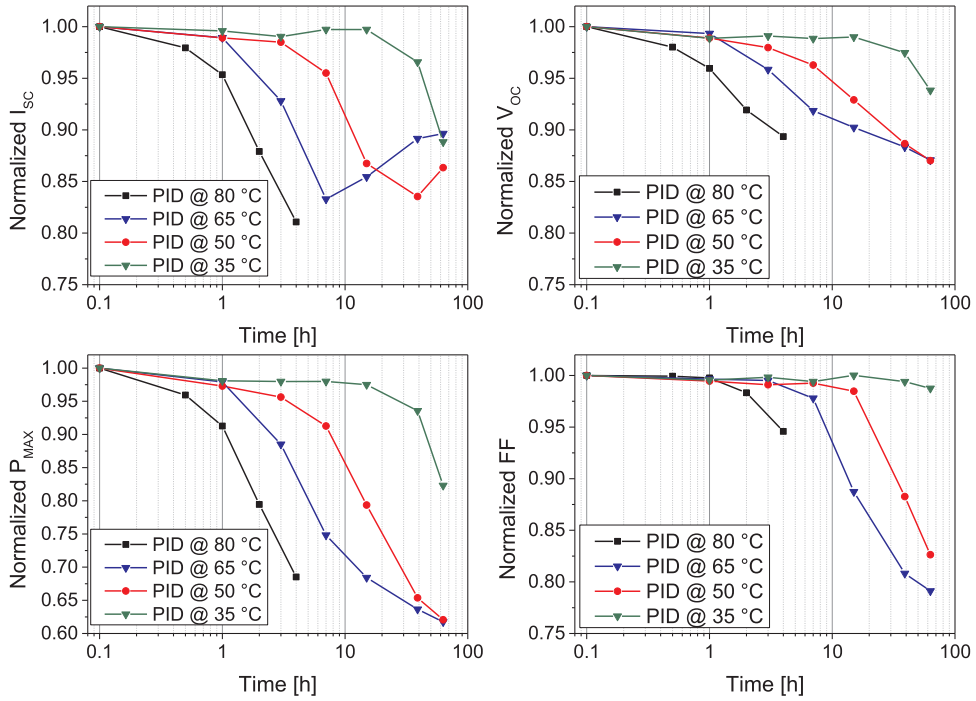

Fig. 6. Evolution of the normalized I_{SC}, normalized V_{OC}, normalized P_{MAX} and normalized FF extrapolated during the PID stresses at different temperatures.

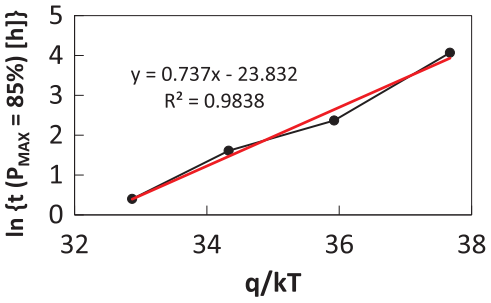

Fig. 7. Arrhenius plot extrapolated from the temperature analysis. The points were extrapolated from the normalized P_{MAX} after the fitting of the power curves.

noticed. The increase of the dark saturation currents can be related to an increase of the recombination inside the pn junction [27]. In fact during the PID stress the degradation of the efficiency conversion can be related to the increase of the surface recombination velocity [17–20].

This will be explained in the Section 4.3 which shows the external quantum efficiency (EQE) analysis during the PID stress.

4.2. Role of the temperature and the voltage: extrapolation of the Arrhenius plot

In this paragraph we present the results obtained on a four cells solar panel subjected to consecutive PID stress and recovery phases with different stress voltages and different stress temperatures. The aim of the procedure is to extrapolate the acceleration factors introduced by the temperature (Arrhenius plot) and by the stress voltage.

The stress procedure is schematically reported in Fig. 5. The solar cells are subjected to PID stress and recovery phases at four different temperatures (35 °C, 50 °C, 65 °C and 80 °C respectively) in order to find the temperature acceleration factor. Then the solar cells are subjected to different PID stress and recovery phase at three different voltages (−300 V, −450 V and −600 V respectively) and constant temperature (65 °C) in order to find the acceleration factor introduced by the stress voltage.

The results of the stress at different temperatures are shown in Fig. 6, which reports the evolution of the normalized I_{SC}, normalized V_{OC}, normalized P_{MAX} and normalized FF for the different stresses. It can be noticed that the degradation kinetics are strongly accelerated by the temperature. The parameters are normalized to the first point of each stress and we ensure that the recovery was higher than 99% at the starting point of each stress.

In order to find the acceleration factor introduced by the temperature, we define as critical time the point where the power is reduced by 15%. The extracted Arrhenius plot is presented in Fig. 7. It can be seen the good accuracy of the fitting. The activation energy of the process is 0.74 eV.

The results of the PID stress at different voltages are shown in Fig. 8, which shows the evolution of the normalized I_{SC}, normalized V_{OC}, normalized P_{MAX} and normalized FF for the different stresses. As can be seen, all the parameters show a reduction with the increase of the voltage. The parameters are normalized to the first point of each stress and we ensure that the recovery was higher than 99% at the starting point of each stress.

In order to find the acceleration factor introduced by the voltage, we define as critical time the point where the power is reduced by 15%. The extracted plot of the time versus the applied voltage is presented in Fig. 9. It can be seen that the time is reduced by a factor of two by increasing the voltage by 150 V.

In order to better understand the physical nature of the degradation, we acquired the electroluminescence images during the stress and recovery phases at different temperatures and voltages. Fig. 10 shows the results. On the first three rows the EL images of the PID stresses @ different voltages are presented (−600 V, −450 V and −300 V for rows #1, #2 and #3 respectively) whereas in the last three rows the EL images of the PID stresses @ different temperatures are depicted (65 °C, 50 °C and 35 °C for rows #4, #5 and #6 respectively). From the analysis of the images we can conclude that (i) the images at 0 h after the recovery (see images inside the red square) are quite similar. This means that the PID degradation is mainly reversible. EL analysis reveals a (minor) permanent degradation that is visible in the bottom cells (see dark regions at the edges of the bottom cells inside the red square); (ii) the final images at 63 h (see images inside the red dashed square) present some dark regions that are responsible of the shunting effect

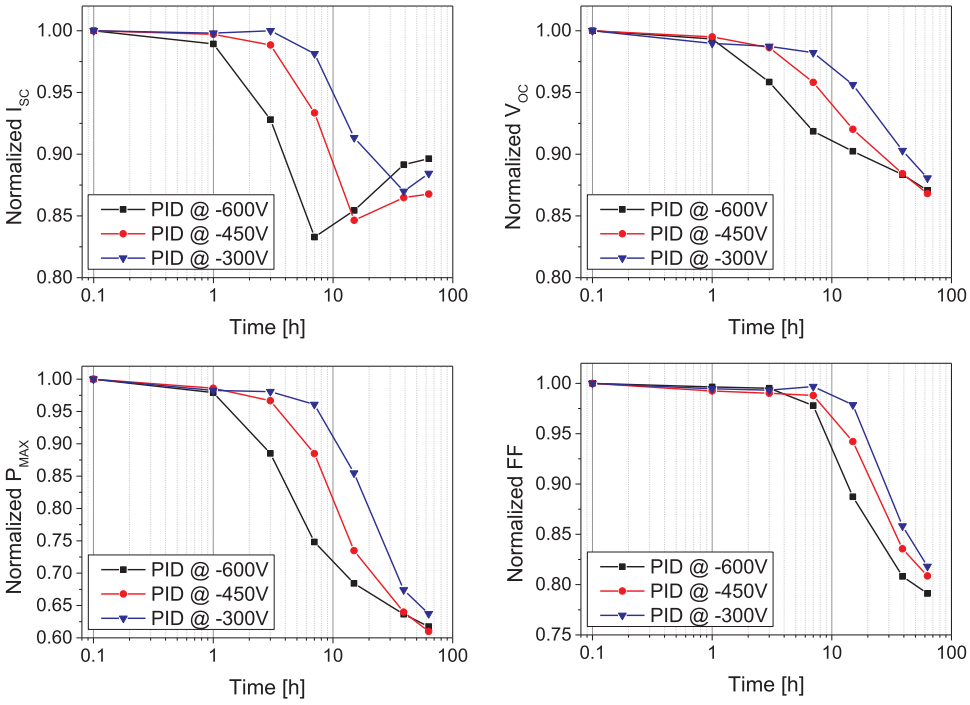

Fig. 8. Evolution of the normalized I_{SC}, normalized V_{OC}, normalized P_{MAX} and normalized FF extrapolated during the PID stresses at different voltages.

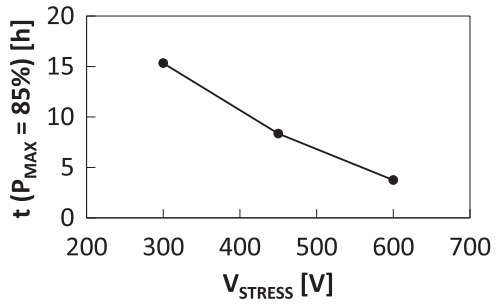

Fig. 9. Acceleration factor introduced by the voltage. The points were extrapolated from the normalized P_{MAX} after the fitting of the power curves.

explained in the paragraph 4.1. In fact the dark regions of the EL images can be associated to a resistive shunt inside the pn junction which cannot generate EL emission during the biasing of the solar cell [28]. This shunting effect is reversible, since after the recovery phases the dark regions disappear. (iii) The accelerating factors introduced by the voltage and temperature, previously calculated from the electrical characterization, are visible also in the EL characterization (see red arrows in Fig. 10). It is worth noticing that the temperature introduces an accelerating factor higher than the voltage.

4.3. Physical origin of PID degradation investigated by electroluminescence and EQE characterization

Fig. 11 presents the electroluminescence analysis and the external quantum efficiency measurement results of a solar cell subjected to PID stress. In Fig. 11a, It can be noticed a first homogeneous darkening of the EL emission up to 15 h and then the appearance of dark regions at 39 h and 55 h. After the first 24 h of recovery @ + 600 V the dark regions disappear and the homogeneous darkness is present only in the center of the solar cell. After 48 h of recovery, the dark region in the center is further reduced.

Fig. 11b and c report the EQE investigation on the same solar cell measured in correspondence to the red squares named “A”, “B” and “C” of the EL images of Fig. 11a.

Two different phenomena were found: (i) the first homogeneous decrease in the EL signal can be related to the reduction of the EQE in the UV-blue region (see solid red arrow in Fig. 11b which shows the EQE of point “A” during the stress and recovery phases). For clarity, in the inset of Fig. 11b we show the evolution of the EQE @400 nm and the EQE @1000 nm during the PID stress. This phenomenon can be related to an increase of the surface recombination velocity due to the migration of the positive Na + ions in the surface layers of the solar cell [19] or to a surface polarization effect [20]. Then (ii) the appearance of dark regions in the EL images cannot be related to any EQE changing (see red circle in Fig. 11c which shows the EQE of points “A” and “B” @ 55 h). This phenomenon can be related to a micro-shunting of the solar cell, which is not revealed by the EQE measurements. The shunting effect is also visible in the electrical characterization previously presented in the Section 4.1 for an EVA-BSC. Fig. 11c shows also the homogeneous recovery of the EL signal in the point “C” (see dashed arrow).

Both phenomena (i and ii) are reversible since, by applying a positive voltage, the EL signal end EQE signal can be recovered (see evolution of point “A” in Fig. 11a and dashed arrow in Fig. 11b). A permanent degradation can be seen from the EL measurements carried out in the edges of the solar cells which show small dark regions like in [21]. The permanent degradation can be due to permanent irreversible phenomena like electro chemical corrosion [29].

For clarity Fig. 12 shows the EQE map at 600 nm overlapped with the EL image after the 24 h of recovery. It can be seen the direct correlation of the EL signal with the EQE measurements. This means that the decreasing of the EQE signal in the UV-blue region can be related to the decrease in the EL signal intensity and the absorption and emission properties of the solar cell are correlated during the first part of the degradation.

4.4. Comparison of front and rear PID

This paragraph shows the comparison of the PID stress carried out with the aluminum sheet in the front side and in the rear side of a 2 × 2 solar module. The encapsulant of the modules was EVA. For clarity Fig. 13 shows the scheme of the two different PID stresses: in the first

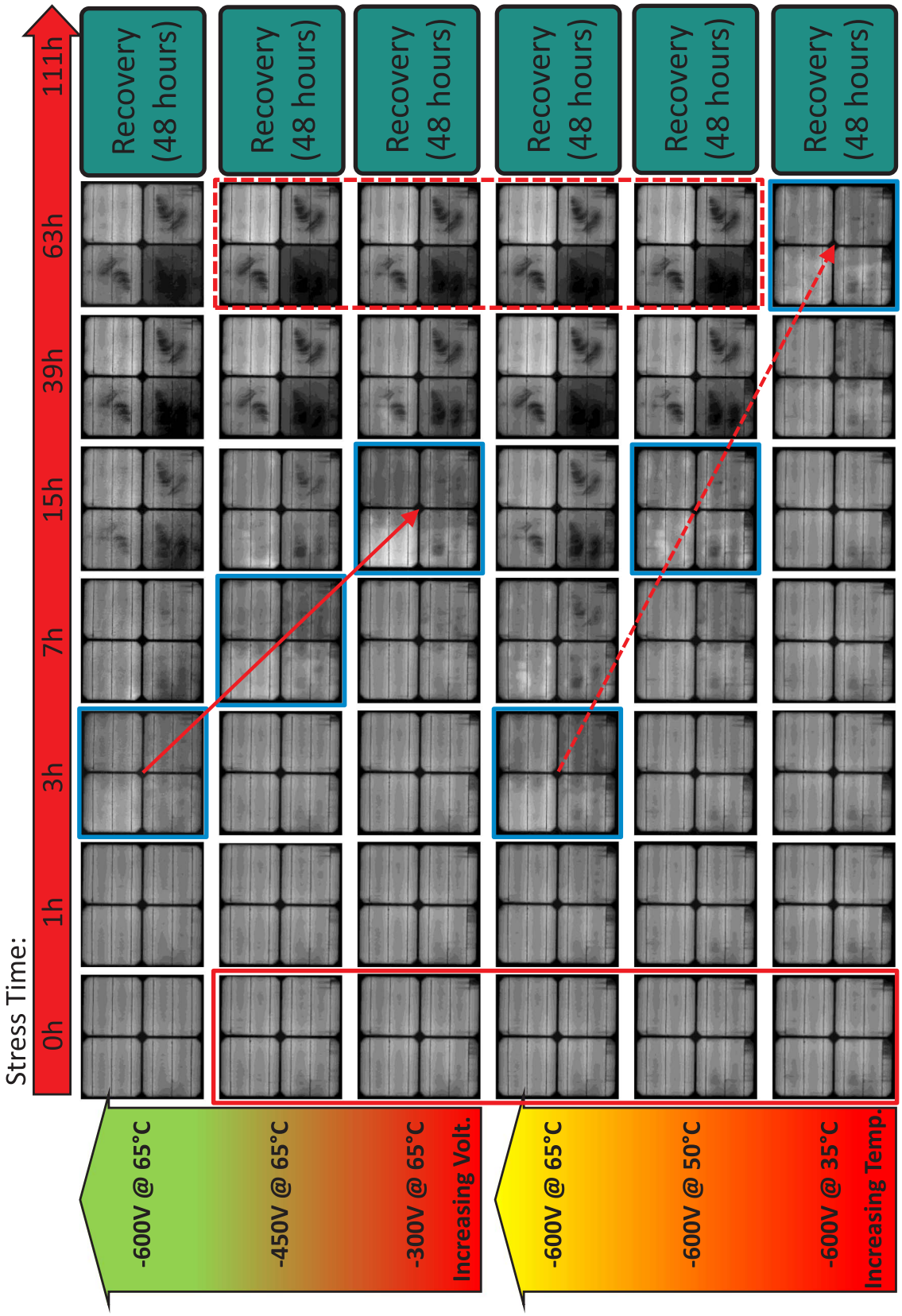

Fig. 10. EL images acquired during the stresses at different temperatures and the stresses at different voltages. The red arrows indicate the accelerating factors introduced by the voltage and the temperature. (For interpretation of the references to color in this figure legend, the reader is referred to the web version of this article).

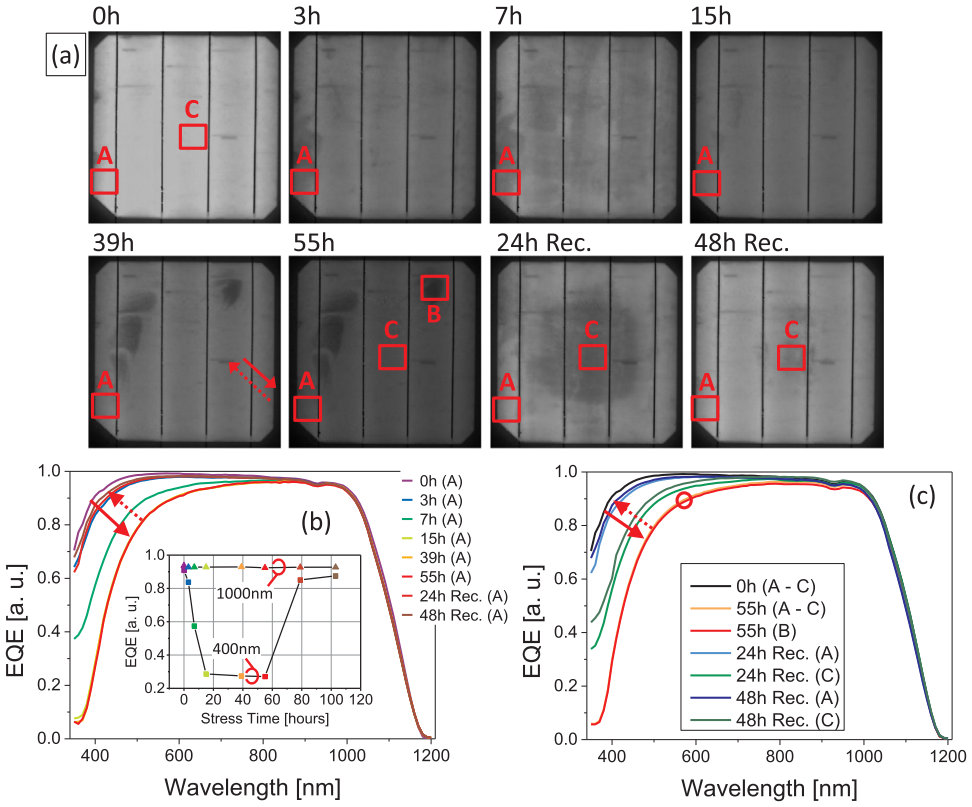

Fig. 11. (a) EL images acquired during the PID stress and (b)-(c) EQE measurements in different positions. (For interpretation of the references to color in this figure, the reader is referred to the web version of this article).

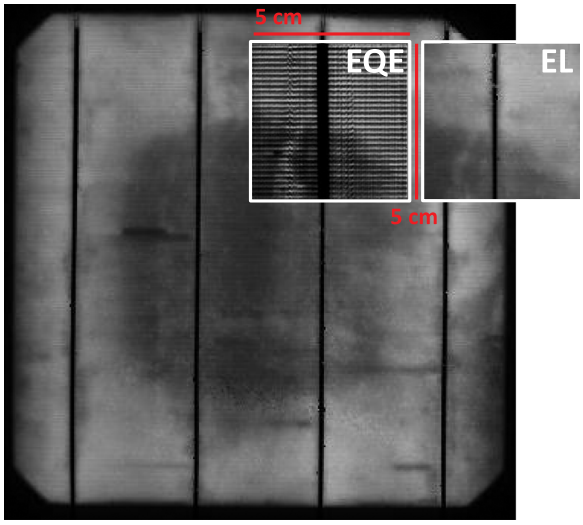

Fig. 12. EL images acquired during the PID stress and QMAP (EQE) measurement in the same region.

case (front side) the front glass and the front encapsulant material are within the uniform electric field generated by the PID stress whereas in the second case (rear side) the rear glass and the rear encapsulant material are within the electric field generated by the PID stress. These two different stress procedures cause the degradation of the front surface layer and rear surface layer respectively.

Fig. 14 shows the comparison of the dark and light IV (@0.7 suns) characterizations during the two different PID stresses: it can be seen that the degradation of the front side PID stress (Fig. 14a–c) is higher than the degradation of the rear side PID stress (Fig. 14d–f).

This can be related to the different degradation induced in the front and rear surfaces of the solar cell. In fact, the cause of the degradation can be related to Sodium migration [19] or to a simple surface polarization effect [20] which both cause an enhancement of the charge recombination velocity [20] in the front or rear surface layers. This can be confirmed by simulations using PC1D simulator and EQE analysis (not shown).

For clarity Fig. 15 shows the evolution of the normalized short circuit current, normalized open circuit voltage, normalized maximum power and normalized fill factor extrapolated during the PID stresses at the rear side and front side of the same solar module. These parameters were extracted from the light IV characterization reported in Fig. 14. As can be noticed, the two PID stresses have different kinetics: the front side stress produces a significantly faster degradation (a time decade) compared to the rear side stress.

This confirms the dependence of PID on the electric field generated by the high voltage, which leads to the ions shift from the external glass toward the solar cell or to a surface polarization effect and, as a consequence, to an increase of the front or rear surface recombination velocity. The optimization of the front layers stack is more complex with respect to the rear one. In fact, the refractive index (RI), the surface sheet resistance (R_{SHEET}) and the anti-reflective coating thickness (T_{ARC}) have to be optimized to ensure good absorption performance. On the other hand, recent studies showed the relation of these parameters (RI, R_{SHEET} and T_{ARC}) with PID-susceptibility [14,30]. In the particular case of the solar cells adopted in this work, the front surface PID causes a higher degradation with respect to the rear one due to the different complexity of the front layers stack.

Possible solutions of the problem are the adoption of different encapsulation materials like POE (see Section 4.1) with a major volumetric resistivity ($> 10^{16}$ [Ω cm]) whit respect to EVA ($> 10^{14}$ [Ω cm]), or the approach of leaving the frame of the solar cell floating. This second technique is not convenient for safety reasons, especially for large-size solar plants where the potential reached by the cells can be in the kV range.

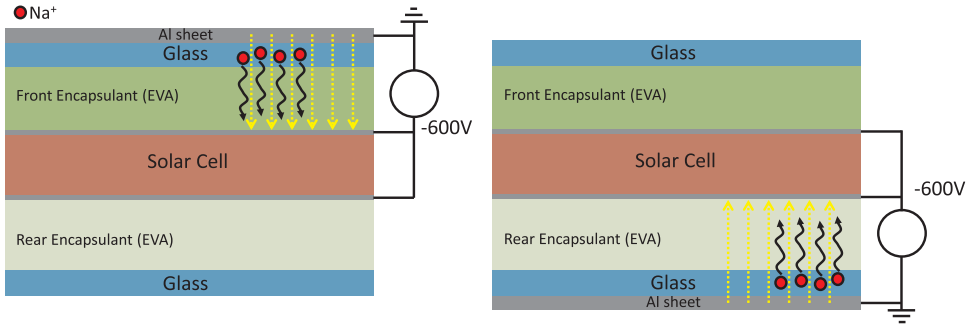

Fig. 13. Physical schemes of the PID stresses executed on the rear and front sides of a solar cell.

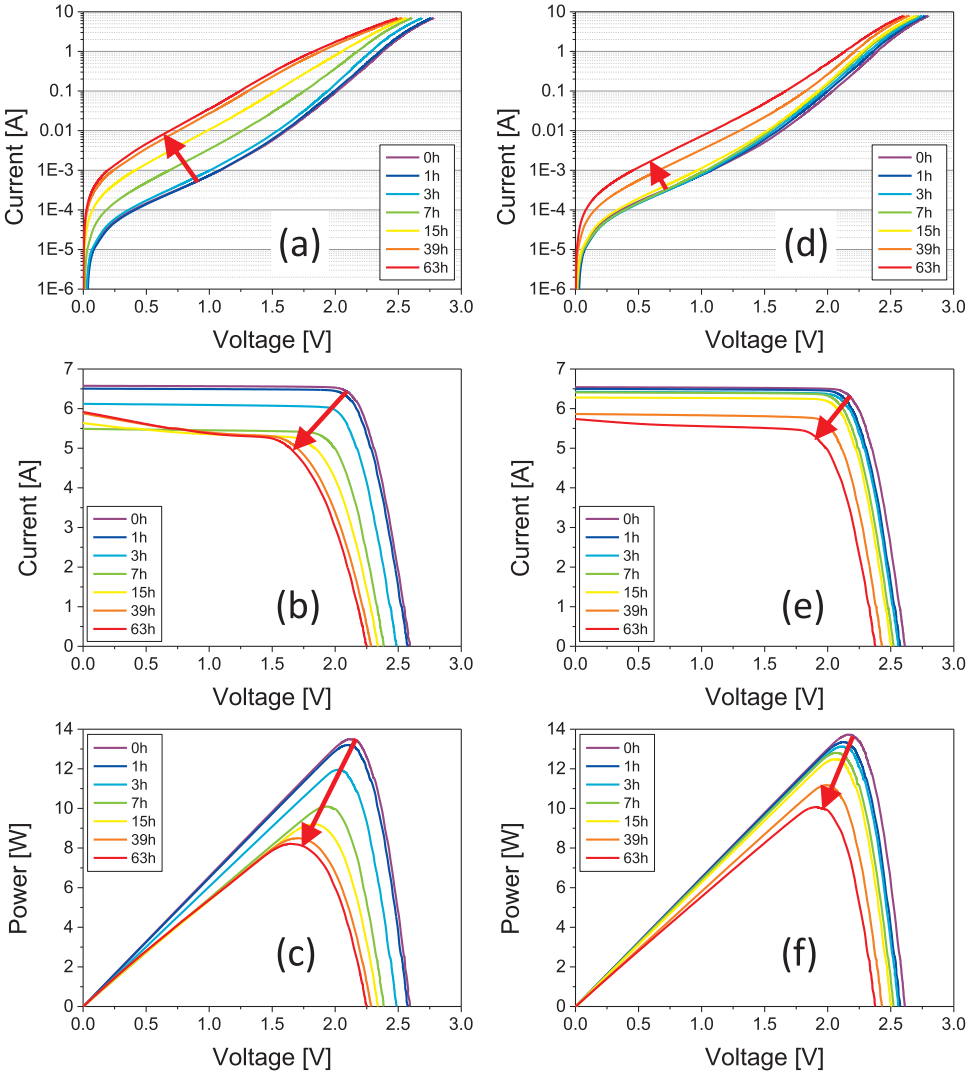

Fig. 14. Dark IV characterization during the front PID stress (a) and during the rear PID stress (d). Light IV and power characterizations @0.7 suns during the front PID stress (b–c) and Light IV and power characterizations @0.7 suns during the rear PID stress (e-f).

5. Conclusions

In this paper, we widely discussed the effects of PID stresses on bifacial n-type silicon solar cells. In particular (i) we showed that the choice of the encapsulant material (EVA and POE) may strongly impact on the robustness to PID. (ii) We analyzed the role of voltage and temperature on the kinetics of the potential induced degradation. In particular we extrapolated the Arrhenius plot from the temperature analysis (35 °C, 50 °C, 65 °C and 80 °C) and the correlation of PID degradation with the applied stress voltage. (iii) The optical analysis (EL and EQE) revealed that the emission of the solar cells is drastically reduced by PID stress. The first decrease in the EL signal can be related to the reduction of the EQE in the UV-blue region, and consequently to the increase of the surface recombination velocity. The final dark regions in the EL images can be related to a shunting effect of the solar cells. Both phenomena are reversible since, by applying a positive voltage, the EL signal is recovered. (iv) The comparison of the rear and front PID stresses revealed that the degradation can be related to positive ions shift from the external glass toward the solar cell or to a simple surface polarization effect. In the particular case of the solar

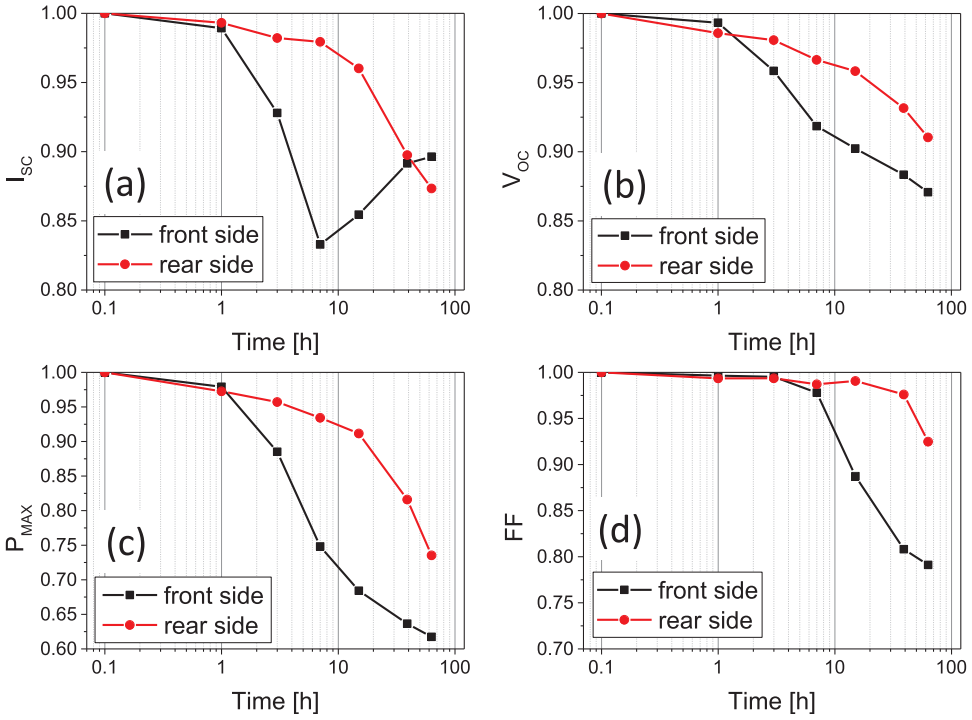

Fig. 15. Evolution of the normalized I_{SC} (a), normalized V_{OC} (b), normalized P_{MAX} (c) and normalized FF (d) extrapolated during the PID stresses executed on the rear and front sides of the solar module.

cells adopted in this work, the front surface PID causes a higher degradation with respect to the rear one due to the different complexity of the front layers stack.

Acknowledgements

Authors would like to acknowledge the Regione Veneto for financing this work, under the project POR - parte FESR “Fondo Europeo Sviluppo Regionale” 2007–2013 azione: 1.1.1 Cod. SMUPR n. 4148. and by ENIAC JU/CALL 2010/270722-2 ERG “Energy for a green society: from sustainable harvesting to smart distribution. Equipments, materials, design solution and their applications”.

References

[1] J.E. Cotter, J.H. Guo, P.J. Cousins, M.D. Abbott, F.W. Chen, K.C. Fisher, "P-Type Versus n-Type Silicon Wafers: prospects for High-Efficiency Commercial Silicon Solar Cells," in, IEEE Trans. Electron Devices 53 (8) (2006) 1893–1901.

[2] R.C.G. Naber, N. Guillevin, A.R. Burgers, L.J. Geerligs, A.W. Weeber, "ECN n-type silicon solar cell technology: An industrial process that yields 18.5%, Photovoltaic Specialists Conference (PVSC), 2009 34th IEEE, Philadelphia, PA, 2009, pp. 990–992.

[3] Xinbo Yang, A. Fell, E. Franklin, Lujia Xu, D. Macdonald, K. Weber, High efficiency n-type silicon solar cells with local back surface fields formed by Laser Chemical Processing, in: Proceedings of the 42nd IEEE Photovoltaic Specialist Conference (PVSC), New Orleans, LA, 2015,pp. 1–4.

[4] F. Kiefer, et al., High efficiency N-type emitter-Wrap-Through silicon solar cells, IEEE J. Photovolt. 1 (1) (2011) 49–53.

[5] C. Gong, et al., Comparison of n- and p-type high efficiency silicon solar cell performance under low illumination conditions, in: Proceedings of the 33rd IEEE, Photovoltaic Specialists Conference, 2008. PVSC '08. San Diego, CA, USA, 2008, pp. 1–4.

[6] A. Metz, et al., International Technology Roadmap for Photovoltaic, ITRPV, Frankfurt, Rep, 1, July 2015.

[7] M. Barbato, A. Barbato, M. Meneghini, A. Cester, G. Mura, D. Tonini, A. Voltan, G. Cellere, G. Meneghesso, Reverse bias degradation of metal wrap through silicon solar cells, Sol. Energy Mater. Sol. Cells 147 (2016) 288–294.

[8] M. Barbato, M. Meneghini, A. Cester, G. Mura, E. Zanoni, G. Meneghesso, Influence of Shunt resistance on the performance of an illuminated string of solar cells: theory, simulation, and experimental analysis, IEEE Trans. Device Mater. Reliab. 14 (4) (2014) 942–950.

[9] F. J. Pern, Factors that affect the EVA encapsulant discoloration rate upon accelerated exposure," Photovoltaic Energy Conversion, Conference Record of the Twenty Fourth. IEEE Photovoltaic Specialists Conference, IEEE First World Conference on vol.1, Waikoloa, HI, 1994, pp. 897-900.

[10] B. Sopori et al., "Understanding light-induced degradation of c-Si solar cells, in: Proceedings of tjhe 38th IEEE Photovoltaic Specialists Conference (PVSC), Austin, TX, 2012, pp. 1115–1120.

[11] Jeanette Lindroos, Hele Savin, Review of light-induced degradation in crystalline silicon solar cells”, Sol. Energy Mater. Sol. Cells 147 (2016) 115–126.

[12] S. Hoffmann, M. Koehl, Effect of humidity and temperature on the potential-induced degradation, Progress. Photovolt.: Res. Appl. 22 (2) (2014) 173–179.

[13] Jaewon Oh, S. Bowden, G. TamizhMani, Potential-induced degradation (PID): incomplete recovery of shunt resistance and quantum efficiency losses, IEEE J. Photovolt. 5 (6) (2015) 1540–1548.

[14] S. Pingel, et al., Potential Induced Degradation of solar cells and panels, in: Proceedings of the 35th IEEE, Photovoltaic Specialists Conference (PVSC), 2010 Honolulu, HI, 2010, pp. 2817–2822.

[15] P. Hacke, et al., Acceleration factor determination for potential-induced degradation in crystalline silicon PV modules, in: Proceedings of the IEEE International, Reliability Physics Symposium, (IRPS) Anaheim, CA, 2013, pp. 4B.1.1-4B.1.5.

[16] J. Kapur, K.M. Stika, C.S. Westphal, J.L. Norwood, B. Hamzavytehrany, Prevention of potential-induced degradation with thin ionomer film, IEEE J. Photovolt. 5 (1) (2015) 219–223.

[17] K. Hara, S. Jonai, A. Masuda, Potential-induced degradation in photovoltaic modules based on n-type single crystalline Si solar cells, Sol. Energy Mater. Sol. Cells 140 (2015) 361–365.

[18] A. Halm, et al., Potential-induced degradation for encapsulated n-type IBC solar cells with front floating emitter, Energy Procedia 77 (2015) 356–363.

[19] V. Naumann, et al., Explanation of potential-induced degradation of the shunting type by Na decoration of stacking faults in Si solar cells, Sol. Energy Mater. Sol. Cells 120 (Part A) (2014) 383–389.

[20] R. Swanson, M. Cudzinovic, D. DeCeuster, V. Desai, Jörn Jürgens, N. Kaminar, W. Mulligan, L. Rodrigues-Barbarosa, D. Rose, D. Smith, A. Terao, K. Wilson, The surface polarization effect in high-efficiency silicon solar cells, in: Proceedings of the International Photovoltaic Science and Engineering Conference, Shanghai, China, January 2005, pp. 410.

[21] V. Naumann, et al., Potential-induced degradation at interdigitated back contact solar cells, Energy Procedia 55 (2014) 498–503.

[22] M. Barbato, M. Meneghini, A. Cester, A. Barbato, G. Meneghesso, Potential induced degradation in high-efficiency bifacial solar cells, in: Proceedings of the IEEE International Reliability Physics Symposium, Pasadena, USA, 17-21 April 2016.

[23] M. Barbato, M. Meneghini, A. Cester, A. Barbato, G. Tavernaro, M. Rossetto, G. Meneghesso, Durability of bifacial solar modules under potential induced degradation: role of the encapsulation materials, in: Proceeding of the European PV Solar Energy Conference and Exhibition, Munich, Germany, 20-24 June 2016.

[24] M. Schwark, et al., Investigation of potential induced degradation (PID) of solar modules from different manufacturers, – in: Proceedings of the 39th Annual Conference of the IEEE Industrial Electronics Society, IECON 2013, Vienna, 2013, pp. 8090–8097.

[25] M. Barbato, et al., Effect of shunt resistance on the performance of mc-Silicon solar cells: a combined electro-optical and thermal investigation, in: Proceedings of the 38th IEEE Photovoltaic Specialists Conference (PVSC), Austin, TX, 2012, pp.

1241–1245.
[26] E.Q.B. Macabebe, V.D.E. Ernest, Parameter extraction from dark current–voltage characteristics of solar cells, S. Afr. J. Sci. 104 (9/10) (2008) 401–404.
[27] D. Lausch, et al., Potential-induced degradation (PID): introduction of a novel test approach and explanation of Increased depletion region recombination, IEEE J. Photovolt. 4 (3) (2014) 834–840.
[28] P. Subinoy Roy, Rajesh Somasundaran, Gupta, Estimation of shunt resistance by electroluminescence imaging, in: Proceedings of the 29th European Photovoltaic Solar Energy Conference and Exhibition, Amsterdam, Netherlands, 22-26 September 2014, pp. 1224–1227.
[29] R.G. Ross Jr., G.R. Mon, L.C. Wen, R.S. Sugimura, "Measurement and characterization of voltage- and current-induced degradation of thin-film photovoltaic modules, Sol. Cells 27 (Issues 1–4) (1989) 289–298.
[30] H. Nagel, A. Metz, K. Wangemann, Crystalline Si solar cells and modules featuring excellent stability against potential induced degradation, in: Proceedings of the 26th Eur. Photovoltaic Solar Energy Conference Exhib. Hamburg, Germany, 2011, pp. 3107–3112.